ISSN 1027-5495. Functional Materials, 29, No.3 (2022), p. 443-450.
doi:https://doi.org/10.15407/fm29.02.443

Effect of surfactant concentration in swift and facile one-pot synthesis of nano-crystalline Cu_2O powder

Chandrashekhar M. Mahajan, Sachin S. Sawant

Department of Engineering Sciences and Humanities, Vishwakarma Institute of Technology, Pune — 411037, Maharashtra, India

Received November 11, 2021

Nanocrystalline Cu_2O powders were synthesized through a facile and swift one pot synthesis in the presence of surfactant polyvinylpyrrolidone (PVP). The PVP solution molarity was varied from 0.4–0.8 mmol before mixing the precursors to investigate its effect on the structure, morphology, and optical properties of Cu_2O nano-crystallites. The XRD analysis confirms the formation of the cubic phase of nanocrystalline Cu_2O by diffraction peaks associated with (110), (111), (200), (220), (311) and (222) crystal planes. The average crystallite size decreases from 23 nm to 14 nm due to an increase in the PVP molarity. In X-ray phase analysis of nanocrystalline powders obtained using solutions of PVP 0.4 mmol and 0.8 mmol, negligible traces of Cu and CuO were found. SEM analysis shows the formation of nanoparticles with decreasing size due to an increase in the PVP molarity. The FTIR spectra show characteristic bands related to molecular vibrations of H–OH stretching, H–OH bending and Cu–O vibration. UV-VIS spectra show an absorption peak around $\lambda = 470$ nm for nano-Cu_2O. The absorption peak shows a blue shift from $\lambda = 472$ nm to $\lambda = 462$ nm with a decrease in the crystallite size due to an increase in PVP concentration. The optical bandgap energy increases from 2.248 eV to 2.519 to 2.772 eV with an increase in the PVP molarity mainly due quantum confinement effects arising from the reduction in crystallite size.

Keywords: Copper oxide, molarity, nanoparticle, optical property, surfactant.

Вплив концентрації поверхнево-активної речовини в швидкому та легкому синтезі нанокристалічного порошку Cu_2O в одному резервуарі. *Ch.M.Mahajan, S.S.Sawant*

Нанокристалічні порошки Cu_2O були синтезовані за допомогою простого та швидкого синінтезу в одному реакторі у присутності поверхнево-активної речовини полівінілпіролідону (ПВП). Молярність розчину ПВП перед змішуванням прекурсорів варіювали від 0,4 до 0,8 ммоль для досліджено його впливу на структуру, морфологію та оптичні властивості нанокристалітів Cu_2O. Рентгенофазовий аналіз підтверджує утворення кубічної фази нанокристалічного Cu_2O з дифракційними піками, пов'язаними з кристалічними площинами (110), (111), (200), (220), (311) та (222). Середній розмір кристалітів зменшується з 23 нм до 14 нм за рахунок підвищення молярності ПВП. Мізерні сліди Cu та CuO були виявлені у рентгенофазовому аналізі для нанокристалічних порошків, отриманих з використанням розчинів ПВП 0,4 ммоль та 0,8 ммоль. Аналіз СЕМ показує утворення наночастинок зі зменшенням розміру при збільшенні молярності ПВП. Спектри FTIR зображують характерні смуги, що відносяться до молекулярних коливань розтягування H–OH, вигину H–OH та коливання Cu–O. Спектри UV-VIS показують пік поглинання близько $\lambda = 470$ нм для нано-Cu_2O. Пік поглинання показує синє зміщення від $\lambda = 472$ нм до $\lambda = 462$ нм із зменшенням розміру кристалітів через збільшення концентрації ПВП. Енергія оптичної забороненої зони збільшується з 2,248 еВ до 2,519 і 2,772 еВ зі збільшенням молярності ПВП, в основному через ефекти квантового обмеження, що виникають через зменшення розміру кристалітів.

1. Introduction

Recently, the scientific community and semiconductor industry have witnessed a renaissance in research related to nanostructured transition metal oxides due to their inherent versatile properties and applications. Copper oxide (Cu_2O) is a promising candidate from transition metal oxide family. It is an abundant, non-toxic, P-type direct band gap (2.2 eV) semiconductor. Literature reports diversified applications of Cu_2O in PeLEDs [1], sensors [2, 3], solar cells [4, 5], Li-ion batteries [6, 7], photocatalysis [8–10], ink for printed electronic devices [11], high performance potassium ion batteries [12], electrocatalytic degradation [13], and antibacterial applications [14]. Cu_2O theoretically has a high efficiency of about 18 % for solar cells [15].

In order to utilize these unique properties of nano Cu_2O, different synthesis approaches have been already explored and wet chemical synthesis methods are quite popular among them [16–18]. It's well-known fact that the synthesis conditions greatly affect the structure and properties of nanomaterials. The literature [16] provides a brief review of various wet chemical synthesis methods for the synthesis of nano-Cu_2O. More recently, the synthesis of Cu_2O on the surface of silica nanoparticles was reported [19], as well as the use of phytochemical synthesis [20].

The wet chemical process parameters like temperature, precursor type and its concentration (i.e., molarity), solvent, surfactant, catalyst — all play a vital role in nano-Cu_2O synthesis. Among them, surfactant is an important parameter which directly affects other precursors, reaction conditions, resultant product in the wet chemical synthesis process. It also affects the size, shape, morphology along with physical properties of the final reaction product. Various surfactants such as sodium dodecyl sulphate (SDS) [21, 22], hexadecyltrimethylammonium bromide (CTAB) [22], and octyl phenyl ether (Triton X-100) [23], and polymers such as polyethylene glycol (PEG) [24] polyvinylpyrrolidone (PVP) [25–29], and regenerated cellulose [21] are used to control particle size, shape, crystalline phase and to stabilize the nanoparticle formation of Cu_2O during wet chemical synthesis.

PVP is a hygroscopic, amorphous, non-toxic, non-ionic, neutral, and water-soluble polymer which also acts as a good stabilizer [27]. PVP, due to its ability to effectively prevent nanoparticle agglomeration, was chosen as a surfactant for facile and swift one-pot nano-Cu_2O synthesis. The present work reports the effect of changing the molar concentration of surfactant (PVP) on the structure, morphology, and optical properties of nano Cu_2O.

2. Experimental

2.1. Materials

In order to obtain nano-Cu_2O through swift one-pot synthesis, the required analytical grade rea-gents like $CuSO_4{:}5H_2O$ (Copper Sulphate Pentahydrate), NaOH (Sodium Hydroxide), the reducing agent $C_6H_8O_6$ (L-Ascorbic Acid) and polyvinylpyrrolidone (PVP) (K30, molecular weight 60000) used as surfactant, were procured from Loba Chemie Pvt. Ltd. Mumbai, Maharashtra, India. These reagents were used for the synthesis without further purification.

2.2 Synthesis method

Nano Cu_2O particles were prepared by a facile, swift and one-pot synthesis technique [28]. First all precursors in approximate stoichiometric proportions (according to reaction requirements): $CuSO_4$ (0.10 mol), NaOH (0.2 mol), $C_6H_8O_6$ (0.1 mol) and PVP surfactant (0.4 mmol, 0.6 mmol, 0.8 mmol) were dissolved in equal volumes of bidistilled water to obtain their aqueous solutions. Then an aqueous solution of PVP was added in the $CuSO_4$ solution; NaOH and $C_6H_8O_6$ solutions were immediately added simultaneously to instantly obtain a yellow-orange precipitate of Cu_2O nanocrystals along with other by-products. The overall reaction representing the synthesis process is shown below.

$$2CuSO_4 + C_6H_8O_6 + 4NaOH \rightarrow$$
$$\rightarrow Cu_2O + C_6H_6O_6 + 2Na_2SO_4 + 3H_2O^{\cdot}$$

The precipitate thus obtained after filtration was thoroughly washed with bidistilled water and then dried in an oven at 60°C to obtain finely ground yellow-orange Cu_2O nanocrystalline powders. Figure 1 shows a flowchart and schematics of various stages of the synthesis process of nanocrystalline Cu_2O powder.

2.3 Characterization

Identification of phase composition, crystal structure and the estimation of average grain size of as synthesized nano-Cu_2O powdered samples was performed by using X-ray diffraction (XRD) analysis using an instru-

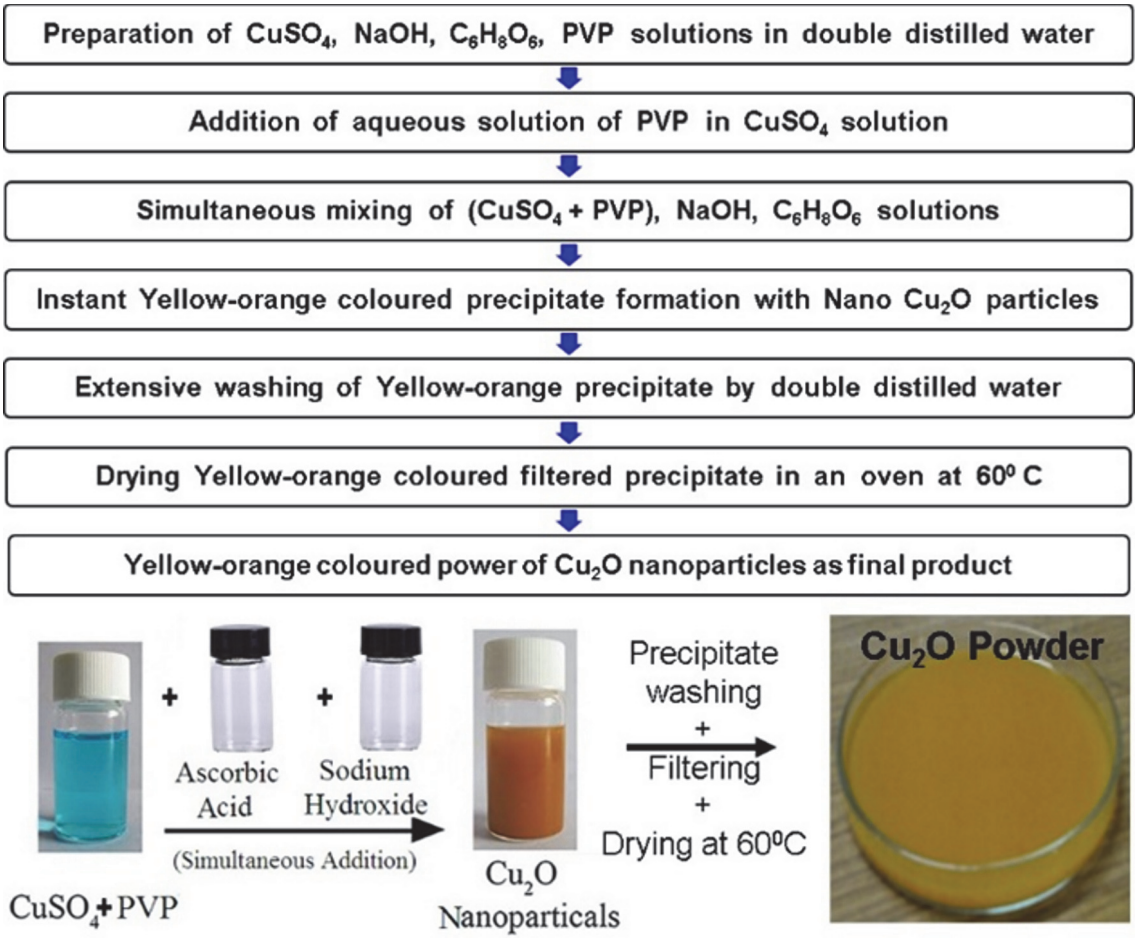

Fig. 1. Flowchart and schematics of steps involved in one-pot synthesis of nanocrystalline Cu_2O powder.

ment (Bruker D-8, Billerica, MA) at 40 kV and 30 mA with a source of CuKα radiation with a wavelength λ = 1.5406 Å. The scanning range was from 20° to 80° and the scan speed was 0.02°/s. Morphological features of the nanocrystalline Cu_2O powder surface were studied with a Field Emission Scanning Electron Microscope (FESEM, JOEL, 7000). To characterize the functional group of Cu_2O nanocrystals, KBr powder was seeded before being subjected to FTIR spectroscopic measurements (manufacturer: Perkin Elmer Spectrum BX, Waltham, MA) in the range of 4000–400 cm^{-1}. Optical absorption measurements of sonicated colloidal dispersions of nanocrystalline Cu_2O samples prepared in doubly distilled water were performed on a UV-VIS spectrophotometric system (Shimatzu 1650PC).

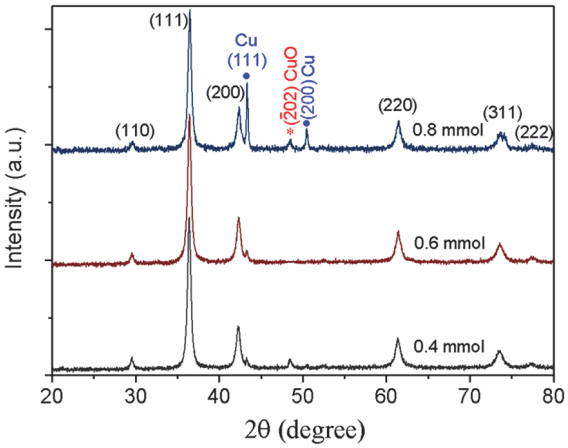

Fig. 2. XRD patterns of Nano Cu_2O particles prepared with varied PVP concentrations.

3. Results and discussion

3.1 Structure and morphology

Figure 2 shows X-ray diffraction patterns of freshly synthesized Cu_2O nanocrystalline powders at molar concentrations of

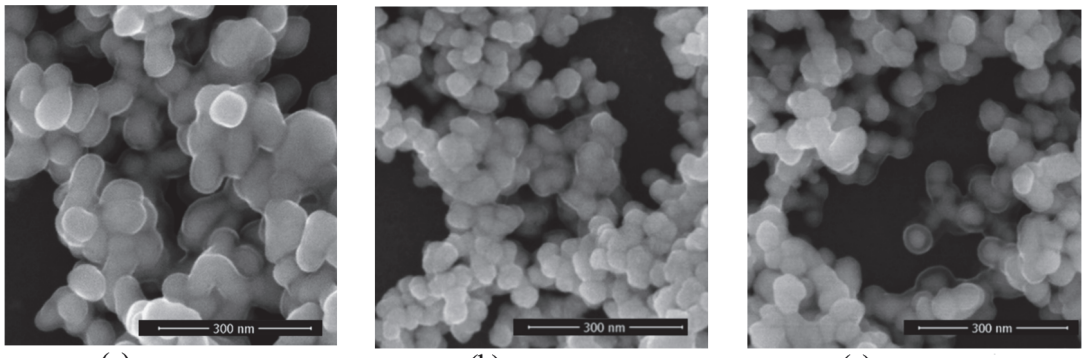

Fig. 3. SEM micrograph of Cu_2O nanocrystalline powder synthesized at different PVP concentrations: (a) 0.4 mmol, (b) 0.6 mmol, (c) 0.8 mmol.

initial PVP solutions of 0.4 mmol, 0.6 mmol, and 0.8 mmol, respectively. It is quite clear that the representative XRD peaks around 2θ angles of 29.56°, 36.4°, 42.34°, 61.44°, 73.54° and 77.38° correspond to (110), (111), (200), (220), (311) and (222) crystal planes respectively. This confirms the Cu_2O cubic phase formation (JCPDS Card No.05-0667). Small traces of the formation of Cu nanoparticles are evident from the XRD peaks at 43.26° for the (111) plane and 50.48° for the (200) plane, as well as at 48.48° for the $(\bar{2}02)$ plane for the CuO phase at lower and higher concentrations of PVP. The full width at half maximum (FWHM) determined from (111) peak for the Cu_2O phase increases with an increase in the PVP molarity indicating a decrease in average crystallite size for the nanocrystalline Cu_2O powder. Thus, an increase in the PVP concentration leads to inhibition of particle growth due to agglomeration; the average crystallite size is suppressed due to the capping effect of surfactants. PVP acts like a capping agent and covers the Cu_2O nano-crystallites during the formation stage thereby preventing further particle growth due to agglomeration. At an increased concentration, PVP will effectively interact with other precursors, thereby inhibiting agglomeration and the formation of large particles.

The Bragg's law (with the first order approximation $n = 1$) helps in estimation of interplanar spacing d for agiven crystal plane characterized by Miller indices (hkl) from wavelength (λ) of X-ray and Bragg's diffraction angle (θ),

$$2d_{hkl}\sin\theta = n\lambda.$$

The average crystallite size (D) of freshly synthesized samples of nanocrystalline Cu_2O powder were calculated by the Scherrer formula [28]

$$D = \frac{k\lambda}{\beta_{(hkl)}\cos\theta},$$

where $k = 0.9$ is the shape factor and $\beta_{(hkl)}$ is full width of the half maxima (FWHM) for a given (hkl) plane. The determined average crystallite sizes were 23 nm, 17 nm and 14 nm for PVP molar concentrations of 0.4 mmol, 0.6 mmol and 0.8 mmol respectively. Thus, an increase in the PVP concentration results in a decrease in the average crystallite size of the Cu_2O nano-powders.

The dislocation density (δ), micro-strain (ε) and lattice constant (a) were estimated from the following relations [29].

$$\delta = \frac{1}{D^2} \qquad \varepsilon = \frac{\beta}{4\tan\theta}$$
$$a^2 = d^2_{(hkl)}(h^2 + hk + k^2)$$

where a is lattice constant. The Cu_2O cubic phase unit cell volume (V) is calculated using formula $V = a^3$.

Table 1 summarises the XRD data with 2θ and $d_{(hkl)}$ values for Cu_2O nanocrystalline powders synthesized at different PVP molarity. Table 2 depicts variations in dislocation density (δ), micro-strain (ε), lattice constant (a) and cell volume (V) with a change in PVP molarity.

The dislocation density increases with an increase in PVP molarity mainly due to a decrease in the average crystallite size. The values of macrostrain, lattice constant and cell volume are in good agreement with literature reports on these parameters [29] and a standard powder diffraction pattern for Cu_2O (JCPDS Card No.05-0667). Figure 3(a), (b) and (c) depicts SEM micrographs

Table 1. 2θ and $d_{(hkl)}$ values from XRD for Cu_2O nano powders synthesized at different PVP molarity

PVP Molarity, mmol	0.4	0.6	0.8
(*hkl*) plane	2θ		
110	29.54°	29.56°	29.66°
111	36.40°	36.40°	36.42°
200	42.24°	42.34°	42.34°
220	61.36°	61.44°	61.44°
311	73.52°	73.54°	73.62°
222	77.30°	77.38°	77.46°
Inter-planar distance (*d*) in Å			
110	3.022	3.020	3.010
111	2.466	2.466	2.462
200	2.138	2.133	2.133
220	1.510	1.508	1.508
311	1.287	1.287	1.286
222	1.233	1.232	1.231

Table 2. Crystallite size (*D*), dislocation density (δ), micro-strain (ε), lattice constant (*a*) and cell volume (*V*) variation for Cu_2O nano powders synthesized at different PVP molarity

PVP Molarity, mmol	0.4	0.6	0.8
Crystallite Size (*D*), nm	23	17	14
Dislocation density (δ)·10^{15}, nm^{-2}	1.89	3.46	5.1
Macrostrain (ε)·10^{-3}, $line^{-2}m^{-4}$	4.78	6.77	8.21
Lattice constant (*a*), Å	4.272	4.272	4.265
Cell volume (*V*), $Å^3$	77.95	77.95	77.58

of Cu_2O nanocrystalline powder samples synthesized at different PVP concentrations: 0.4 mmol, 0.6 mmol and 0.8 mmol respectively. Figure 3(a) shows the formation of large sized, agglomerated Cu_2O nanocrystals with uneven size distribution. The crystal size varies from 30 nm to 100 nm. Figure 3(b) clearly shows fine, less agglomerated Cu_2O nanocrystals of completely cubic morphology with an average size of less than 30 nm. Further, Fig. 3(c) depicts the formation of smaller sized Cu_2O nanocrystallites with an average size around 20 nm. Here, a higher concentration

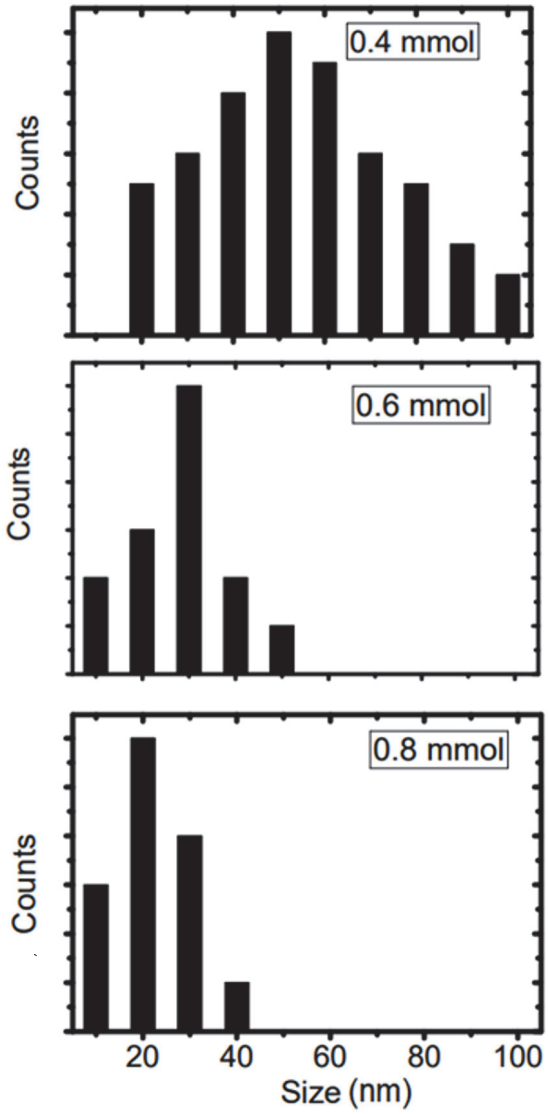

Fig. 4. Crystallite size (nm) distribution in Cu_2O nanocrystalline powder samples synthesized at different PVP concentrations.

of PVP resulted in inhibition of agglomeration and thus reduced particle size.

Figure 4 depicts the variation in crystallite size for the Cu_2O powders synthesized at different PVP concentrations. It is clear from the SEM images that the particle size distribution is quite uneven for the powder synthesized using 0.4 mmol PVP solution, and becomes sparse and narrow with 0.6 mmol and 0.8 mmol PVP solutions.

3.2 Chemical composition studies

Chemical composition of freshly synthesized Cu_2O nanocrystalline powder samples was investigated by FTIR analysis. Figure 5 shows FTIR spectra of Cu_2O nanocrystalline

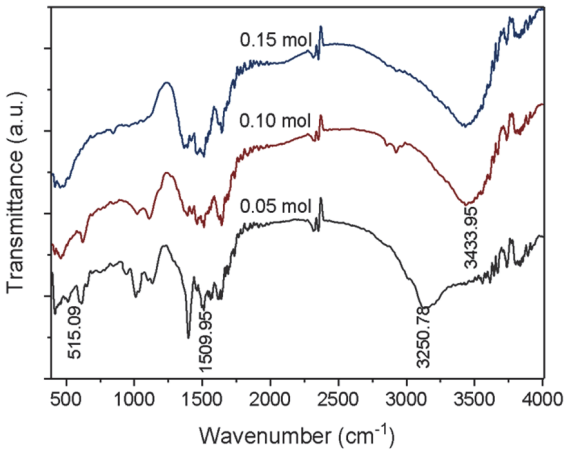

Fig. 5. FTIR spectra of Cu_2O nanocrystalline powders synthesized at different PVP concentrations: 0.4 mmol, 0.6 mmol and 0.8 mmol.

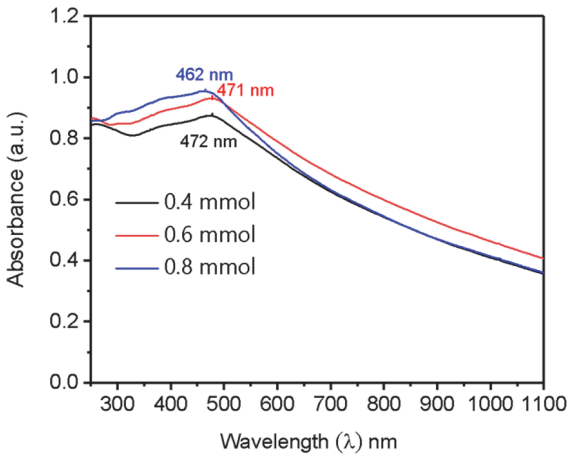

Fig. 6. UV-VIS spectra of Cu_2O nano-crystallites synthesized at different PVP concentrations: 0.4 mmol, 0.6 mmol and 0.8 mmol.

powders synthesized at different PVP concentrations: 0.4 mmol, 0.6 mmol and 0.8 mmol.

These samples showed wide absorption bands located around 3433.95 cm^{-1} and ascribed to the H–OH stretching mode. Also, a small band corresponding to the H–OH bending mode is observed around 1509.95 cm^{-1}. Further, for Cu_2O phase, the characteristic Cu–O vibrational mode [30] can be observed in the region of the wavenumber of 515.09 cm^{-1}. Table 3 shows the modes of molecular vibrations depending on the wavenumber, which appear in the FTIR spectra for Cu_2O nanoparticles synthesized at various PVP concentrations.

3.3 Studies of optical properties

Figure 6 shows the measured UV-VIS spectra in the range of λ from 250 nm to 1100 nm for Cu_2O nanocrystalline powder samples synthesized at PVP concentrations of 0.4 mmol, 0.6 mmol and 0.8 mmol respectively. Figure 6 also shows the presence of the characteristic absorption peaks around λ = 472 nm (0.4 mmol), λ = 471 nm (0.6 mmol) and λ = 462 nm (0.8 mmol) respectively, thereby confirming the formation of Cu_2O nanoparticles [24, 28–33]. A blue shift for the characteristic absorption peaks with an increase in the PVP molar concentration is clearly evident from Fig. 6. This shift of the absorption peak mainly results from the size variation of the Cu_2O nanoparticles due to a change in the surfactant molar concentration. Thus, an increase in the surfactant concentration inhibits agglomeration of Cu_2O nano-crystallites during the synthesis.

The calculations of the optical band gap (E_g) for Cu_2O nano-crystallites synthesized at different PVP molarities: 0.4 mmol, 0.6 mmol, 0.8 mmol were carried out using the Tauc relation [34] given by (2).

$$\alpha h\nu = (h\nu - E_g)^n \quad . \tag{2}$$

Here, the terms α, h, ν and $h\nu$ respectively means an absorption coefficient, Planck constant, frequency and the energy of the incident photon. The exponent n can take on any of the values 1/2, 1/3, 2 and 3/2 which determines the type of electronic transition that caused the absorption. Since

Table 3. The modes of molecular vibrations and their locations in the FTIR spectrum for Cu_2O nanocrystalline powders synthesized at different PVP concentrations.

Molecular vibrational modes	PVP Molar Concentration, mmol		
	0.4	0.6	0.8
	Wavenumber, cm^{-1}		
H–OH Stretching	3250.78	3433.95	3442.43
H–OH Bending	1508.35	1509.95	1511.33
CuO Vibrational	512.34	515.09	510.95

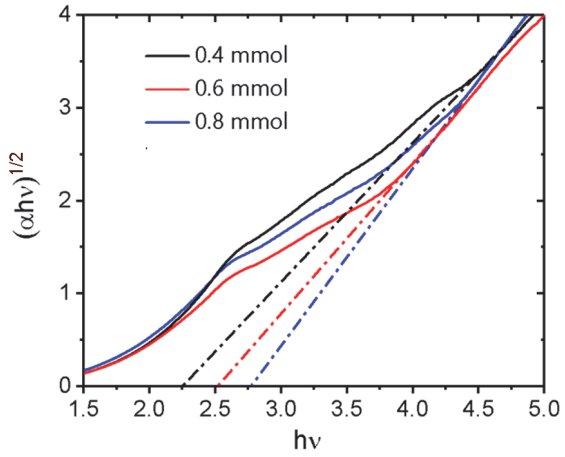

Fig. 7. The plot of $(\alpha h\nu)^{1/2}$ vs $h\nu$ for nano-crystalline Cu_2O synthesized at different PVP concentrations: 0.4 mmol, 0.6 mmol, 0.8 mmol.

the optical band gap for a direct band gap semiconductor is due to a direct allowed transition, in this case, the best linear relationship was obtained by plotting $(\alpha h\nu)^{1/2}$ against $h\nu$.

Figure 7 represents the plot of $(\alpha h\nu)^{1/2}$ vs $h\nu$ for Cu_2O nano-crystallites synthesized at different PVP molarities: 0.4 mmol, 0.6 mmol and 0.8 mmol. The direct band gap (E_g) of these samples was measured using the Tauc relation and found to vary from 2.248 eV for the 0.4 mmol PVP sample to 2.519 and 2.772 eV for the 0.6 mmol and 0.8 mmol PVP samples, respectively. These E_g values were higher than the theoretical value of 2.2 eV for bulk Cu_2O due to nanoparticle sizes which subsequently leads to quantum confinement [12–15]. Thus, an increase in PVP concentration reduced agglomeration, which is associated with a decrease in particle size, and therefore, increased the band gap E_g, which can be understood from the blue shift.

4. Conclusions

The effect of polyvinylpyrrolidone (PVP) surfactant on the structure, morphology and optical properties of Cu_2O nano-crystallites obtained using a facile and swift one-pot synthesis was successfully investigated. XRD analysis established the formation of Cu_2O nano-crystallites with estimated average grain sizes varying in the range from 50 nm to 15 nm with an increase in the PVP molarity. SEM analysis has shown transition from cubical to spherical morphology for Cu_2O nano-crystallites with an increase in the PVP molarity. The FTIR spectra show the presence of characteristic bands related to molecular vibrations, which confirms the formation of nanocrystalline Cu_2O. UV-VIS spectra show a strong intense absorbance peak located near $\lambda = 470$ nm and attributed to nano Cu_2O. Its position also varies from $\lambda = 472$ nm to $\lambda = 462$ nm due to a decrease in the crystallite size with an increase in PVP concentration. The measurements using Tauc plots reveal an increase in optical band gap energy values from 2.248 eV to 2.519 and to 2.772 eV with increasing PVP molarity due to grain size reduction and quantum confinement. Thus, the molarity of PVP surfactant is one of the key criteria affecting the size, morphology and optical properties of nano-crystalline Cu_2O synthesized using this method.

Acknowledgement. The authors wish to thank for the support extended by the Management, Director, Vishwakarma Institute of Technology.

References

1. R.Chakraborty, H.Bhunia, S.Chatterjee, A.Pal, *J. Solid State Chem.*, **281**, 121021 (2020).
2. S.Singh, U.Kumar, B.Yadav et al., *Results Phys.*, **15**, 102772 (2019).
3. Y.Zhao, H.Liu, L.Shi et al., *Sens. Actuators B*, **315**, 128155 (2020).
4. T.Miyata, H.Tokunaga, K.Watanabe et al., *Thin Solid Film*, **697**, 137825 (2020).
5. D.Osorio-Rivera, G.Torres-Delgado, R.Castanedo-P?rez et al., *Mater. Res. Bull.*, **122**, 110669 (2020).
6. Y.Ren, X.He, W.Sui et al., *J. Mater. Res. Technol.*, **9**, 8081 (2020).
7. Y.Wang, L.Cao, J.Li et al., *Chem. Eng.*, **391**, 123597 (2020).
8. V.Spiridonov, X.Y.Liu, S.Zezin et al., *J. Organomet. Chem.*, **914**, 121180 (2020).
9. N.Omrania, A.Nezamzadh-Ejhieh, *J. Photoch. Photobio. A*, **389**, 112223 (2020).
10. F.Zhang, Y.Li, M.Qi et al., *Appl. Catal. B*, **268**, 118380 (2020).
11. M.Mallik, S.Moniaa, M.Gupta et al., *J. Alloy Compd.*, 829 (2020).
12. Ji Ma, C.Liu, *J. Colloid Interface Sci.*, **594**, 352 (2021).
13. S.Mao, X.Sun, H.Qi, Z.Sun, *Sci. Total Environ.*, **793**, 148492 (2021).
14. A.Zheng, S.Sabidi, T.Ohno et al., *Chemosphere*, **286 Part 2**, 131731 (2022).
15. Y.Liu, H.Turley, J.Tumbleston et al., *Appl. Phys. Lett.*, **98**, 162105 (2011).
16. S.S.Sawant, A.D.Bhagwat, C.M.Mahajan, *J. Nano-Electron. Phys.*, **8**, 01035 (2016).
17. Y.Bai, T.Yang, Q.Gu et al., *Powder Technol.*, **227**, 35 (2012).
18. L.Gau, C.Murphy, *Nano Lett.*, **3**, 231 (2003).

19. J.Prajapati, D.Das, S.Katlakunta et al., *Inorganica Chim. Acta*, **515**, 120069 (2021).
20. M.Mannarmannan, K.Biswas, *Chemistry Select*, **6**, 3534 (2021).
21. W.Huang, M.Lyu, Y.Yang, M.Huang, *J. Am. Chem. Soc.*, **134**, 1261 (2012).
22. H.Kuo, H.Huang, *J. Phys. Chem. C.*, **112**, 18355 (2008).
23. F.Luo, D.Wu, L.Gao et al., *J. Cryst. Growth.*, **285**, 534 (2005)
24. L.Gou, C.Murphy, *J. Mater. Chem.*, **14**, 735 (2004).
25. Y.Sui, W.Fu, H.Yang et al., *Cryst. Growth Des.*, **10**, 99 (2010).
26. A.Mishra, D.Pradhan, *Cryst. Growth Des.*, **16**, 3688 (2016).
27. S.Jadhav, D.Nikam, V.Khot et al., *New J. Chem.*, **37**, 3121 (2013).
28. S.S.Sawant, A.D.Bhagwat, C.M.Mahajan, *J. Nano- Electron. Phys.*, **8**, 01036 (2016).
29. S.S.Sawant, C.M.Mahajan, *J. Nano-Electron. Phys.*, **14**, 02011 (2022).
30. R.D.Prabu, S.Valanarasu, V.Ganesh et al., *Surface and Interface Analysis*, **50**, 346 (2018).
31. A.Mahmoud, K.Al?Qahtani, S.Alfaij et al., *Sci. Rep.*, **11**, 12547 (2021).
32. Y.Bai, T.Yang, Q.Gu et al., *Powder Technol.*, **227**, 35 (2012).
33. L.Gau, C.Murphy, *Nano Lett.*, **3**, 231 (2003).
34. R.Swarnkar, S.Singh, R.Gopal, *Bull. Mater. Sci.*, **34**, 1363 (2011).